

# Faraday waves in 2:1 internal resonance

By DIANE M. HENDERSON AND JOHN W. MILES

Institute of Geophysics and Planetary Physics, University of California, La Jolla,  
CA 92093, USA

(Received 23 October 1989)

Experiments are reported on Faraday waves in a circular cylinder, which are internally resonant with either the subharmonic mode (with frequency  $\frac{1}{4}$  that of the forcing) or the superharmonic mode (with frequency equal to that of the forcing). For subharmonic resonance both modes achieved comparable amplitudes that were steady, or were modulated with one or two periods, or exhibited quasi-periodic or chaotic motions. A stability map of these responses is presented. Theoretical predictions of linear stability and growth rates are tested. Measurements of steady amplitudes, limit-cycle frequencies and wave slopes at breaking are presented. Some of the measured phase-plane trajectories are shown to have theoretical counterparts. For superharmonic resonance the amplitude of the superharmonic was never comparable with that of the Faraday wave. For low modes an energy exchange occurred during the initial period of growth, and a precession instability sometimes developed. For high modes for which both frequencies and wavenumbers are in a 2:1 ratio, superharmonic resonance occurred irreproducibly; it appeared to be overwhelmed by 1:1 interactions among the possible Faraday-wave modes.

---

## 1. Introduction

We consider here internal resonances between a Faraday wave, the standing wave that is subharmonically excited by the vertical oscillation of a cylinder of fluid, and either its subharmonic (which has a frequency equal to  $\frac{1}{4}$  that of the forcing) or its superharmonic (which has a frequency equal to that of the forcing). For the circular cylinder of radius  $R = 3.72$  cm used in our experiments, the type of resonance that occurs depends on the fluid depth, such that, in addition to the constraint implied by the 2:1 frequency ratio, the wavenumbers satisfy certain kinematic conditions. A 2:1 resonance is possible between the (0, 1)-mode wave and its subharmonic, the (1, 0) mode, for a fluid depth of  $h = 0.76$  cm. We investigated this configuration in detail and found that subharmonic resonance does exist and is robust. In particular, we measured threshold forcing amplitudes for neutral stability and linear growth rates, which we compare with the theoretical predictions of Becker & Miles (1986). We also measured the hysteretic neutral stability curve and stability curves delineating modal amplitudes that exhibited threshold behaviour, steady-state behaviour, breaking, single-period limit cycles, double-period limit cycles, quasi-periodicity, and chaos. We found the amplitudes of the steady-state waves, the slopes of waves at breaking, the frequencies of the limit cycles of waves modulated with a single period, and the largest Lyapunov exponent for waves exhibiting chaos.

A 2:1 resonance is possible between the (0, 1)-mode Faraday wave and its superharmonic, the (0, 3)-mode, for  $h = 1.15$  cm. We measured time series of these two modes, which did not display the rich dynamics present in the subharmonic case. We also searched for superharmonic resonance between a pair of modes for which the

wavenumber and frequency of the superharmonic are, respectively, twice those of the fundamental (cf. Wilton's ripple for progressive waves).

The evolution equations governing the subharmonic resonance case are isomorphic to those describing an internally resonant double pendulum that is forced at four times the frequency of the dominant mode. Becker & Miles (1986) analysed this system and found the fixed points of the equations, local stability, Hopf bifurcations, and chaos. The corresponding analysis of the equations for the Faraday-wave problem, which are given in Miles & Henderson (1990), follow directly. Superharmonic resonance has been examined by Miles (1984), Gu & Sethna (1987) and others. (See Miles & Henderson (1990) for a review of superharmonic resonance in Faraday waves.) Miles (1984) examined perfectly tuned superharmonic resonance and found steady-state solutions with no Hopf bifurcations possible. Gu & Sethna (1987) allowed for detuning and found that Hopf bifurcations are possible in some parametric regimes. However, these regimes correspond to damping rates that are much smaller than those observed in the present experiments. No limit cycles or chaotic motions are theoretically possible when damping rates are comparable with those observed in our experiments.

We proceed as follows. In §2 we first present the kinematic conditions for 2:1 resonance between standing waves in circular cylinders, including the role of linear viscous damping in determining the normal modes. We then recapitulate the theoretical predictions of Becker & Miles (1986) for subharmonic resonance and relate them to Faraday waves. In §3 we briefly describe the experimental apparatus and procedures, emphasizing those aspects that differ from the description in Henderson & Miles (1990).

In §4 we present the results of experiments on subharmonic resonance. Predictions of Becker & Miles (1986) for the neutral stability of the Faraday wave agree reasonably well with our data. The measured, hysteretic neutral stability curve is lower than the non-hysteretic curve for Faraday-wave frequencies  $f$  smaller than the natural frequency  $f_2$  and joins the non-hysteretic curve for  $f > f_2$ . (Simonelli & Gollub (1989) observed this phenomenon for single-mode Faraday waves in a square cylinder.) The measured, linear growth rates were generally larger than predicted. After about ten minutes of evolution time, the experiments exhibited a variety of wave responses that depended on the forcing parameters. Steady-state waves had amplitudes that were larger than those predicted by the weakly nonlinear theory of Becker & Miles (1986). Those waves that exhibited single-period limit cycles had modulation frequencies qualitatively consistent with, although less than, those predicted at the Hopf bifurcation. The slopes of waves on the boundary between breaking and steady-state amplitudes varied linearly with the deviation of the frequency of the Faraday wave from that of the natural frequency. Some of the measured attractors in phase space are similar to two of the attractors obtained numerically in Becker & Miles (1986) and herein.

In §5 we present the results of experiments on superharmonic resonance. We found evidence of a resonance in the transient stage of evolution following the initial Faraday-wave growth for superharmonic resonance between low modes. The two modes evolved out of phase (unlike the non-resonant case, for which they are in phase) until they reached either a steady state or a precession instability similar to that observed by Gollub & Meyer (1983) for high-mode Faraday waves. For the high mode Wilton's-ripple case, we found some evidence of resonance, but it occurred irreproducibly. In general, it appeared that superharmonic resonance was obscured by the many possible 1:1 resonances among modes with frequencies near that of the

Faraday wave but with different wavenumbers. Resonance of this type has been observed by Ciliberto & Gollub (1985). For both the low-mode and the high-mode cases, the amplitude of the superharmonic mode remained an order of magnitude smaller than that of the Faraday wave, as also was true in the non-resonant case.

In the Appendix we examine the Wilton's-ripple case for (high-mode) waves in a rectangular cylinder. We found no evidence of superharmonic resonance. Although many different (spatial) modes were possible that had the same natural frequency, the one-dimensional mode was usually the one excited. As in the circular cylinder, the superharmonic mode never attained an amplitude comparable to that of the Faraday wave.

## 2. Theory

For 2:1 resonance there must exist two normal modes with frequencies  $\omega_1$  and  $\omega_2$ , such that  $\omega_2 \sim 2\omega_1$ . Here and throughout, the single subscript is an abbreviation for the pair of numbers associated with each mode. A subscript 1 indicates the fundamental mode; a subscript 2 indicates its superharmonic. The frequencies of the normal modes are related to the corresponding wavenumbers by the dispersion relation

$$\omega_{lm} = (1 - \delta_{lm}) \tilde{\omega}_{lm} = (1 - \delta_{lm}) [(gk_{lm} + Tk_{lm}^3) \tanh k_{lm} h]^{\frac{1}{2}}, \quad (1)$$

where  $\tilde{\omega}_{lm}$  is the inviscid natural frequency of the  $(l, m)$  mode,  $k_{lm}$  is the corresponding wavenumber,  $h$  is the water depth,  $T$  is the kinematic surface tension, and  $\omega_{lm}$  is the frequency decreased by Stokes boundary-layer damping, where  $\delta_{lm} = \gamma_{lm}/\omega_{lm}$  is the ratio of actual to critical damping, and  $\gamma_{lm}$  is the linear damping rate. (Expressions for  $\delta_{lm}$  are available from Miles (1967), but see §3 for a discussion of the damping rates used herein.)

For a circular cylinder of radius  $R$ ,  $l$  and  $m$  indicate the number of nodal diameters and nodal circles, respectively, and  $k_{lm}$  is the  $m$ th positive zero of  $J_l'(k_{lm}R)$  (where  $J_l'$  is the derivative of the  $l$ th-order Bessel function). The resonance condition on wavenumbers is either  $l_2 = 2l_1$  or  $l_2 = 0$ ; i.e. the normal mode of the superharmonic either has twice as many nodal diameters as the fundamental or has zero nodal diameters. No restriction applies to the number of nodal circles of each mode or to the relationship of the magnitudes of the wavenumbers. For a cylinder of fixed radius, superharmonic resonances are possible for a continuum of fluid depths. For details, see Tadjbakhsh & Keller (1960) for resonance in gravity waves and Concus (1962) for capillary-gravity waves. Becker & Miles (1991) show that resonance also exists for some modes in infinite depths.

To obtain the evolution equations for the modes participating in subharmonic resonance, we follow Miles (1984; see also Miles & Henderson 1990) and expand the surface displacement in the form

$$\eta(r, \theta, t) = \sum_{n=1}^{\infty} \eta_n(t) \psi_n(r, \theta), \quad (2)$$

where the  $\psi_n$  form a complete set of orthogonal modes ( $\psi_0 = \text{constant}$  is ruled out by conservation of mass),

$$\eta_n(t) = l_n [p_n(\tau) \cos n\omega t + q_n(\tau) \sin n\omega t] \quad (n = 1, 2), \quad (3)$$

are the corresponding generalized coordinates,  $\tau \equiv \epsilon\omega t$  is a slow time, the forcing frequency is  $4\omega$ ,

$$\epsilon = \alpha_0 k_2 \tanh k_2 h \quad (4)$$

is a small parameter ( $\epsilon \ll 1$  implies weak nonlinearity), and

$$l_2 = \frac{4\epsilon a_1}{a_{211} - 4a_{112}} = l_1 \left( \frac{a_1}{2a_2} \right)^{\frac{1}{2}} \quad (5a)$$

are the lengthscales of the dimensionless amplitudes  $p_n$  and  $q_n$ , where

$$a_i = (k_i \tanh k_i h)^{-1}, \quad (5b)$$

$$a_{lmn} = C_{lmn} [1 + \frac{1}{2}(k_l^2 - k_m^2 - k_n^2) a_m a_n], \quad (5c)$$

$$C_{lmn} = \frac{1}{S} \iint \psi_l \psi_m \psi_n \, dS, \quad (5d)$$

and  $S$  is the cross-sectional area. For subharmonic resonance, here and in §4, the normal mode of the Faraday wave is indicated by the subscript 2, while the normal mode of its subharmonic is indicated by the subscript 1. The normal modes for the present experiments on subharmonic resonance are

$$\psi_2 = N_2 J_0(k_{01} r), \quad \psi_1 = N_1 J_1(k_{10} r) \cos \theta, \quad (6a, b)$$

where  $k_2 \equiv k_{01}$ ,  $k_1 \equiv k_{10}$ ,

$$N_2 = \frac{1}{J_0(k_{01} R)}, \quad N_1 = \left[ \frac{2}{(k_{10} R)^2 - 1} \right]^{\frac{1}{2}} \frac{k_{10} R}{J_1(k_{10} R)}. \quad (6c, d)$$

The evolution equations for the fundamental and Faraday modes are

$$\dot{p}_1 + \alpha_1 p_1 = -\beta_1 q_1 - p_2 q_1 + p_1 q_2, \quad (7a)$$

$$\dot{q}_1 + \alpha_1 q_1 = \beta_1 p_1 - p_1 p_2 - q_1 q_2, \quad (7b)$$

$$\dot{p}_2 + \alpha_2 p_2 = -\beta_2 q_2 + 2q_2 + p_1 q_1, \quad (7c)$$

$$\dot{q}_2 + \alpha_2 q_2 = \beta_2 p_2 + 2p_2 - \frac{1}{2}(p_1^2 - q_1^2), \quad (7d)$$

where

$$\beta_n = \frac{(n\omega)^2 - \omega_n^2}{2\epsilon n\omega^2} \quad (8)$$

is a tuning parameter (the sign of which is opposite that in Becker & Miles 1986), and  $\alpha_n = n\delta_n/\epsilon$  is a damping parameter.

The linear growth rate for the  $k_2$  (Faraday) mode, which ultimately loses stability to the  $k_1$  mode, is found by setting  $p_1 = q_1 = 0$  for small times, and solving for  $p_2$  and  $q_2$ . For initial times,  $p_2, q_2 \sim \exp(\epsilon\omega\gamma_G t)$ , where

$$\gamma_G = -\alpha_2 + (4 - \beta_2^2)^{\frac{1}{2}}. \quad (9)$$

No growth, or  $\gamma_G = 0$ , implies neutral stability, and the threshold amplitude at which the subharmonic waves with frequency  $f_2$  are excited is

$$a_0 = [k_2 \tanh(k_2 h)]^{-1} \left[ \delta_2^2 + \frac{(4\omega^2 - \omega_2^2)^2}{(2\omega)^4} \right]^{\frac{1}{2}}. \quad (10)$$

Becker & Miles (1986) obtain (7) from their analysis of a double pendulum. Here we recapitulate the results of their local stability analysis from which they obtain the criterion for stability of the plane surface, the fixed points for the wavefields, the location in parameter space of the Hopf bifurcations, and the frequencies of the resulting limit cycles at the Hopf bifurcations. In terms of Faraday waves, the plane surface is stable if

$$\gamma \equiv \alpha_2^2 + \beta_2^2 - 4 > 0 \quad (11)$$

(which is (9) with  $\gamma_G = 0$ ). If (11) is not satisfied, the waves grow and achieve the following steady-state (dimensional) amplitudes. The amplitude of the Faraday wave is

$$a_2 = l_2 N_2 (p_2^2 + q_2^2)^{\frac{1}{2}} = l_2 N_2 (\alpha_1^2 + \beta_1^2)^{\frac{1}{2}}, \quad (12)$$

and that of its subharmonic is

$$a_1 = l_1 N_1 (p_1^2 + q_1^2)^{\frac{1}{2}} = \sqrt{2} l_1 N_1 (\beta_1 \beta_2 - \alpha_1 \alpha_2 \pm [4(\alpha_1^2 + \beta_1^2) - (\alpha_1 \beta_2 + \alpha_2 \beta_1)^2]^{\frac{1}{2}})^{\frac{1}{2}}. \quad (13)$$

The necessary and sufficient conditions for the stability of these waves are

$$4E_1 + \gamma + 4\alpha_1 \alpha_2 > 0, \quad 2E_1 \left( \frac{\alpha_2}{\alpha_1} + 1 \right) + \gamma > 0, \quad (14a, b)$$

and 
$$D \equiv 2E_1 (\gamma + 4\alpha_1 \alpha_2) + \frac{\alpha_1 \alpha_2 \gamma^2}{(\alpha_1 + \alpha_2)^2} + 4 \left( \alpha_1^2 + \beta_1^2 + \frac{\alpha_1^2 \alpha_2}{\alpha_1 + \alpha_2} \right) \gamma > 0, \quad (14c)$$

where 
$$E_1 = \frac{1}{2}(p_1^2 + q_1^2), \quad E_2 = (p_2^2 + q_2^2) \quad (15a, b)$$

are the non-dimensional energies of each mode. A Hopf bifurcation occurs when  $D$  is negative. The frequency of the resulting limit cycle is given by

$$f_*^2 = (2\pi)^{-2} \left[ 2E_1 + \frac{\alpha_1 \gamma}{\alpha_1 + \alpha_2} \right]. \quad (16)$$

Miles (1984) gives the analogous development for superharmonic resonance. Here we need only consider the threshold amplitude for neutral stability, which is given by

$$a_0 = [k_1 \tanh(k_1 h)]^{-1} \left[ \delta_1^2 + \frac{(\omega^2 - \omega_1^2)^2}{4(\omega)^4} \right]^{\frac{1}{2}}, \quad (17)$$

where, here and in §5, the subscript 1 indicates the normal mode of the Faraday wave, a 2 indicates the normal mode of its superharmonic, and the forcing frequency is  $2\omega$ . We also note that the superharmonic resonance,  $\epsilon \equiv a_0 k_1 \tanh k_1 h$ .

### 3. Experimental apparatus and procedures

The experimental apparatus is the same as that described by Henderson & Miles (1990). It consisted of a circular (radius = 3.72 cm) glass cylinder oscillated vertically by a Bruel & Kjaer Electromagnetic shaker. A VAXstation II provided the command signal for all experiments except for measurements of the hysteresis curve, for which a Textronix FG 501A function generator provided command. A non-contacting proximity sensor created a signal proportional to the cylinder motion. A servo-controller compared this signal to the command signal and constantly corrected the cylinder motion to follow that programmed. The fluid was distilled water filtered of organics and particles greater than 0.2  $\mu\text{m}$  with Kodak Photo Flo 200 solution added in the ratio of 80:1 (water to Photo Flo), such that the surface tension, measured with a Fisher Model 20 tensiometer, was 42.3 dyn/cm at 23 °C.

The (effective) viscosity of the fluid was calculated from equations (2.19)–(2.21) of Henderson & Miles (1990), using the measured, linear decay rates. For the experiments on subharmonic resonance, the effective viscosity of  $\nu = 0.010 \text{ cm}^2/\text{s}$  inferred from this calculation agreed with the value for clean water. The effective value for low-mode superharmonic resonance was  $\nu = 0.016 \text{ cm}^2/\text{s}$ . For high-mode superharmonic resonance, we could not measure the damping rates of the superharmonic modes directly (the upper limit for our damping measurements was

10 Hz). Hence, we used the value for the lower modes (at the appropriate depth) of  $\nu = 0.030 \text{ cm}^2/\text{s}$ . (See Henderson & Miles (1990) for a discussion of damping measurements.) The effective viscosity depended on the fluid depth; however, regardless of its value, the decay rate was linear and provided reasonable agreement between predicted and measured natural frequencies.

In the experiments on subharmonic resonance we found that the depth had to be monitored carefully. The depth was not critical for the occurrence of the subharmonic resonance; however, reproducibility of the depth was critical for reproducible results. The bottom of the circular cylinder was nearly flat with the centre raised about 0.01 cm. The fluid evaporated at a maximum rate of about 0.002 mm/h. (This rate was not constant; it varied from hour to hour and was usually much less than 0.002 mm/h.) As a consequence, no one measurement could require more time than about thirty minutes, after which time we measured the depth in the centre of the cylinder (accurate to  $\pm 0.02 \text{ mm}$ ), and added fluid accordingly until  $h = 7.60 \text{ mm}$ . A Lory Type C point gauge in conjunction with a dial micrometer accurate to 0.01 mm was used to measure the depth. We cleaned the cylinder and changed the fluid every two hours because experiments performed after this period were sometimes irreproducible. This irreproducibility could have been a consequence of temporal changes in the surface-film or of fallout that settled on the bottom of the cylinder.

To measure the neutral stability curve, we fixed the forcing frequency (known to  $10^{-6} \text{ Hz}$ ) and varied the forcing amplitude  $a_0$ , using the VAXstation II for the command signal. For each  $a_0$  the wavemaker was started from rest and given five minutes to excite a wave. In this way, we converged upon a threshold forcing amplitude to  $\pm 0.005 \text{ mm}$ . A Textronix FG 501A function generator provided the command signal for measurements of the threshold hysteresis curve. Again, for a fixed frequency (known to  $10^{-2} \text{ Hz}$ ), we varied the forcing amplitude. We started with an  $a_0$  for which a wave was present and decreased it until the wave died. In measuring the hysteresis curve, we found that for  $f$  much less than  $f_2$ , the waves tended to break and that breaking of a few minutes duration entrapped small air bubbles into the fluid, which rendered the results irreproducible. Hence, we cleaned the cylinder and added fresh fluid after each experiment involving breaking waves.

Surface displacements were measured with an *in situ* capacitance probe with a diameter of 1.15 mm. For experiments on resonance between the (0, 1)- and (1, 0)-modes in the circular cylinder, the gauge was 4 mm from the endwall, in the point of maximum displacement of the (1, 0)-mode; hence, the gauge location depended on the orientation of the (1, 0)-mode; see §4.2. We filtered the gauge signal at 25 Hz with a low-pass analog filter and digitally sampled it at 50 Hz with the computer. We determined linear growth rates by starting the wavemaker from rest and measuring the slope of the linear portion of the growing amplitude curve.

For experiments on superharmonic resonance, we subtracted the cylinder motion from the time series before further analysis. For resonance between the (0, 1)- and (0, 3)-modes, the gauge was in the centre of the circular cylinder. For resonance between the (7, 1)- and (0, 8)-modes, it was off-centre, at the point of maximum fluid displacement. For the high-mode experiments, we low-pass filtered the signal at 100 Hz and digitally sampled it at 200 Hz. For all experiments, we complex-demodulated the signal at the two frequencies of interest to obtain the envelope time series of the amplitudes and phases of each mode. (See Bloomfield 1976, pp. 118–150 for a discussion of complex demodulation.)

We measured the long-term behaviour of the (0, 1)–(1, 0) subharmonic resonance discussed in §4.2 as follows. We chose a grid of points throughout the measured linear

stability space of forcing amplitude versus Faraday-wave frequency. The computer limited the resolution in forcing frequency to about 0.02 Hz, or 0.01 Hz for the Faraday wave and the stability space. We arbitrarily chose the resolution in forcing amplitude to be about 0.035 mm. We started the wavemaker from rest with parameters corresponding to a point on the grid. For some experiments, especially near the threshold, the wave required five minutes to grow initially. The (0, 1)-wave grew first and became unstable to the (1, 0)-wave. We measured time from the point at which this instability first occurred. After the waves evolved for five minutes, we took a 5 min, 32 s time series with 16600 points at 50 Hz. We monitored the water depth after every one or two experiments, depending on the time required for the initial growth of the Faraday wave. This procedure provided measurements, consistent throughout stability space, of the long-term behaviour of the wave fields, and also allowed time to monitor the water depth and to fix the forcing amplitude precisely. We then classified the response as discussed in §4.2. We emphasize then, that by ‘long-term’ evolution, we mean that at the end of our time series the wave field had evolved for ten minutes and thirty-two seconds, or about 2400 Faraday wave periods.

#### 4. Results of subharmonic resonance

In this section we present the results from experiments in which a (0, 1)-mode Faraday wave with frequency  $f$  resonated with its subharmonic, the (1, 0)-mode. Table 1 lists the parameters for the normal modes. We report the behaviour of the wave field first for initial times of evolution, and second for long-term evolution. Note that, in this section, a subscript of 2 signifies the normal mode of the Faraday wave; a subscript of 1 signifies the normal mode of its subharmonic; and the forcing frequency approximates  $2f_2 = 4f_1$ .

##### 4.1. Linear behaviour

Figure 1 shows the predicted and measured neutral stability curves for the excitation of the (0, 1)-mode. The frequency of the minimum of the neutral stability curve corresponds to the natural frequency  $f_2$  of the Faraday wave. The predicted natural frequency is 4.10 Hz, about 0.8% less than the measured value of 4.135 Hz. The predicted threshold amplitudes (10) agree fairly well for  $f < f_2$  and overpredict amplitudes for  $f > f_2$ . The predicted, minimum threshold amplitude of 0.263 mm is about 9% higher than the measured value of 0.240 mm. Note that the (0, 1)-mode invades the stability space of the predicted (3, 0)-mode. This result contrasts with our earlier experiments on the neutral stability of single-mode Faraday waves (Henderson & Miles 1990) and with the experiments on superharmonic resonance discussed in §5, in which the theory correctly predicts the excitation of the (3, 0)-mode. Figure 1 also shows the measured hysteresis curve obtained as described in §3. The hysteresis and neutral stability curves coalesce at the minimum point, a result also observed by Simonelli & Gollub (1989), and are about the same for  $f > f_2$ . We note that for  $f < f_2$  the usual scenario for hysteresis was present; the (steady) wave amplitudes decreased with decreasing forcing amplitude. However, for  $f > f_2$  the waves exhibited large modulations whose amplitudes and periods changed with decreasing forcing amplitude. These more complicated dynamics may have caused the convergence of the neutral stability and hysteresis curves in our experiments.

Figure 2 shows the measured and predicted growth rates of the (0, 1)-mode when the forcing amplitude was 0.352 mm. The error bars indicate the standard deviation

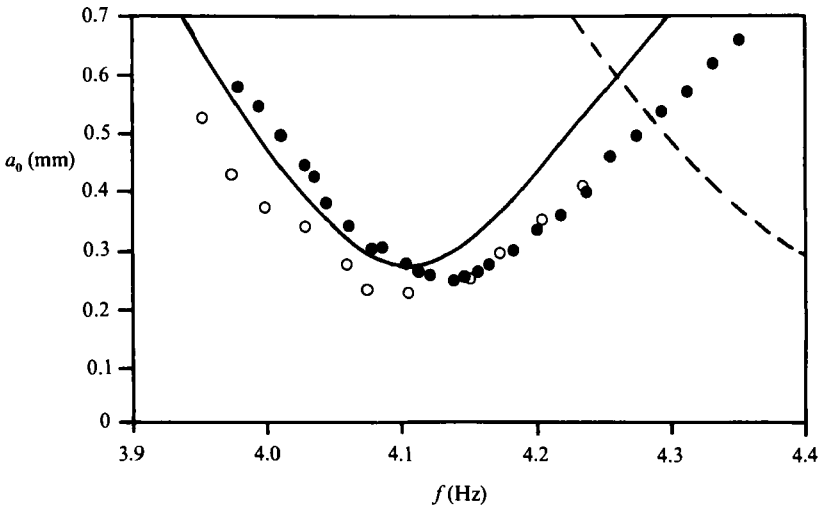


FIGURE 1. Stability space of forcing amplitude as a function of the (0, 1)-mode Faraday-wave frequency for  $h = 0.760$  cm. —, predicted neutral stability curve for the (0, 1)-mode; ●, measured neutral stability curve; ○, measured hysteresis curve; ---, predicted neutral stability curve for the (3, 0)-mode with  $k_{30} = 1.13$  rad/cm.

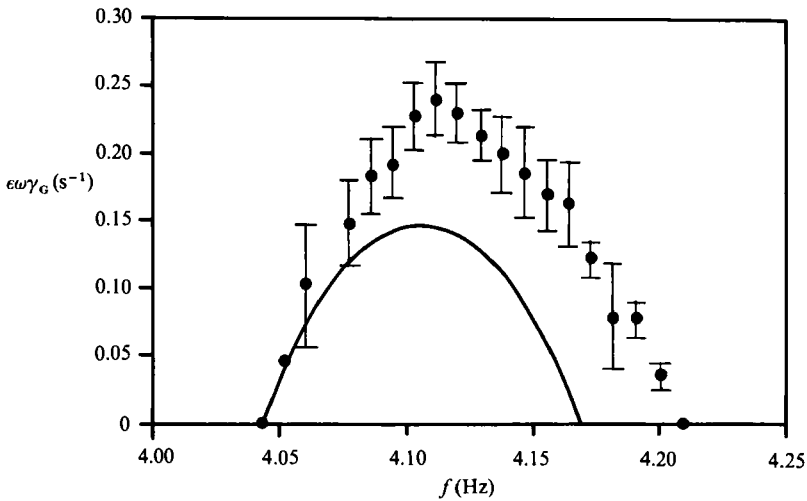


FIGURE 2. Linear growth rates of the (0, 1)-mode Faraday wave as a function of its frequency for  $h = 0.760$  cm. —, predictions; ●, measurements.

$h$ (cm)	$k_2/(\text{mode})$ (rad/cm)	$f_2$ (Hz)	$\delta_2$	$k_1/(\text{mode})$ (rad/cm)	$f_1$ (Hz)	$\delta_1$	$\nu^{\text{effective}}$ (cm <sup>2</sup> /s)
0.76	1.03 (0, 1)	4.10	0.018	0.49 (1, 0)	2.05	0.027	0.010

TABLE 1. Parameters and normal modes for the experiments on subharmonic resonance. The subscript 2 indicates the parameter appropriate for the normal mode of the Faraday wave. The subscript 1 indicates the parameter appropriate for the normal mode of its subharmonic.

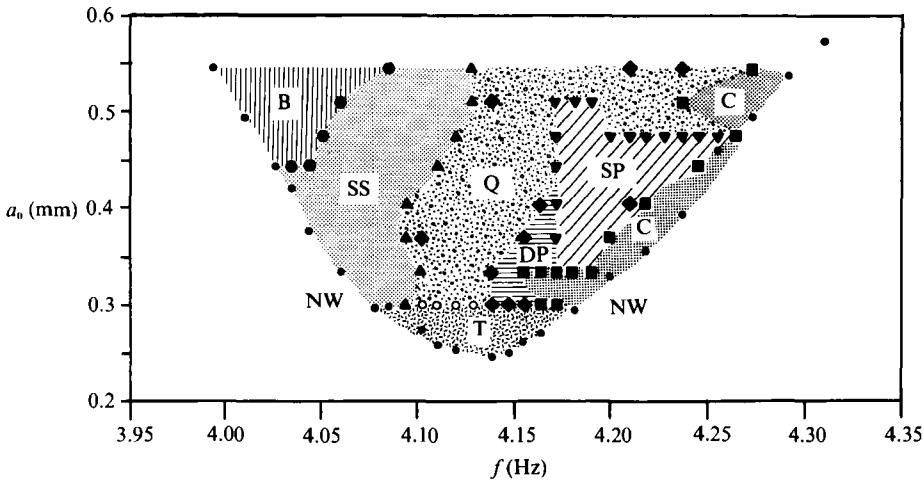


FIGURE 3. Measured stability space of forcing amplitude as a function of Faraday-wave frequency for the long-term behaviour of the subharmonic resonance between the (0, 1)- and (1, 0)-modes with  $h = 0.760$  cm. Each region marks a different type of wave response: NW, no waves; B, breaking waves; SS, steady-state amplitudes; Q, quasi-periodic amplitudes; T, threshold behaviour; SP, single-period amplitude modulations; DP, double-period amplitude modulations; C, chaotic amplitude modulations. Symbols represent the locations of experiments that provide boundaries between the regions. The four diamonds inside the Q region and the one inside the SP region are locations of wave fields with double-period amplitude modulations (in addition to the ones that occurred in the DP region).

for each experiment. Contact-line effects and defects in the glass walls were presumably responsible for these large deviations. The measured growth rate near the natural frequency is about 1.6 times larger than predicted. This discrepancy is probably due, at least in part, to the neglect (in the theory) of higher-order terms in wave amplitude. We note that the growth of the (0, 1)-wave was indeed linear for about the first 75% of its growth, with the rate presented in figure 2; the rate usually increased slightly for about the final 25% of the wave's growth. The initial growth of the (1, 0)-mode began when the Faraday wave had achieved a maximum amplitude. Its growth was not linear and was about five times that of the Faraday wave.

#### 4.2. Nonlinear behaviour

In this section we discuss the long term behaviour, represented in figure 3, of the Faraday wave and its subharmonic. There the small circles along the region marked NW (for no waves) are the data points shown as solid circles in figure 1. They separate regions in which no waves were excited from those in which waves were excited. We identified the behaviour of the waves after excitation by the regions shown above the small circles. Each region is separated from its neighbours by symbols that represent the locations of boundary experiments in this stability space. We have shown only the locations of the experiments that delineate the borders and have not included the location of experiments throughout the regions within these borders. However, one can see the resolution in frequency by the symbols at the top of the T region and the resolution in forcing amplitude by the column of triangles along the left border of the SP region. As described in §3, we examined the wave field evolution for about ten minutes. Hence, figure 3 represents a snapshot of stability space after about ten minutes of wave-field evolution. We do not believe it would change significantly after another five or ten minutes of wave evolution, but

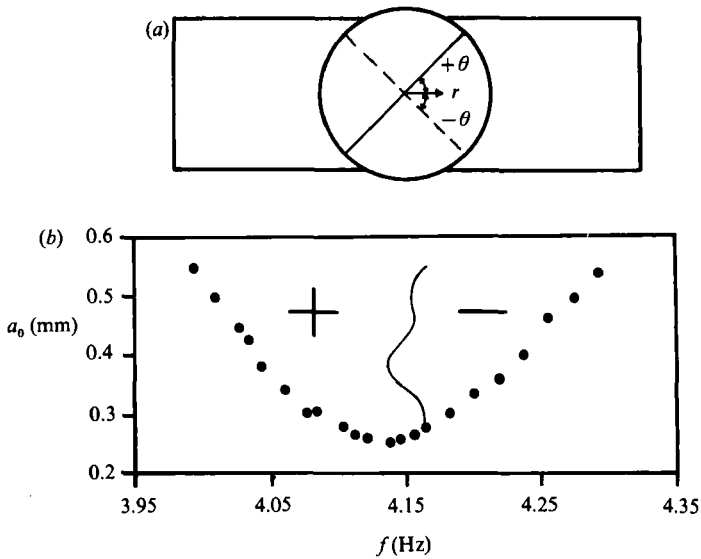


FIGURE 4. Most common orientations of the (1, 0)-mode. (a) Schematic plan view of the circular cylinder on its support; —, orientation with  $+\theta$ ; ---, orientation with  $-\theta$ . (b) Location in stability space of the boundary —, between the  $+\theta$  and  $-\theta$  orientations for the experiments represented in figure 3.

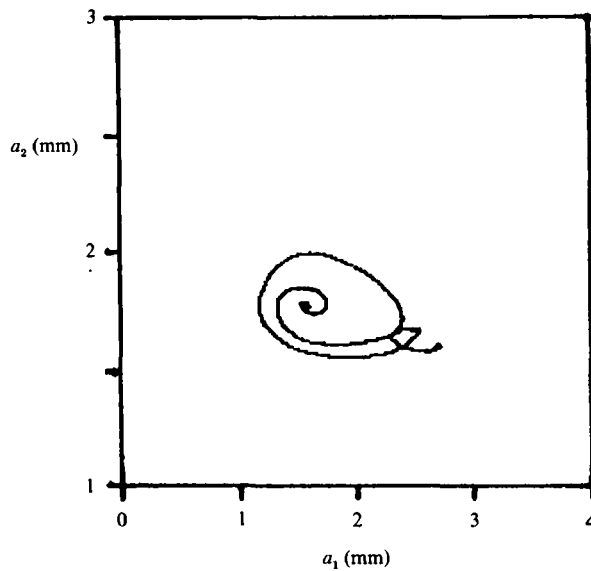


FIGURE 5. Phase space of the amplitude of the (0, 1)-mode as a function of the amplitude of the (1, 0)-mode;  $f_{0,1} = 4.078$  Hz,  $a_0 = 0.442$  mm.

evaporation might induce significant changes after half an hour or more. We remark that, for the most part, the orientation of the (1, 0)-mode was constant throughout a particular experiment (after an initial transient); exceptions included some wave fields in the threshold and chaos regions. Figure 4(a) shows a plan view of the circular cylinder with the two most common orientations of the (1, 0)-mode relative to the cylinder support. For most of the experiments  $\theta$  was about  $45^\circ$ . Figure 4(b) shows the observed orientation for the experiments in §4.2. The plus and minus orientations are

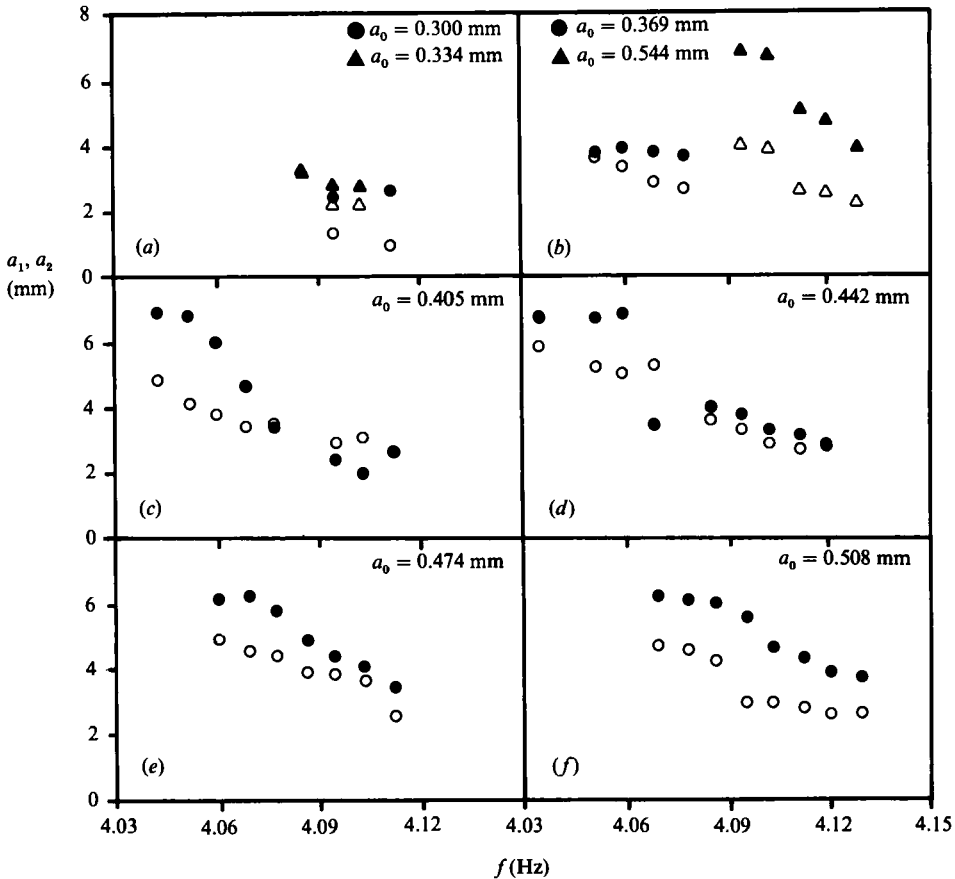


FIGURE 6. Measured steady-state amplitudes of the wave fields from the SS region as a function of Faraday-wave frequency for the different forcing amplitudes as indicated. The solid symbols represent  $a_1$ , the amplitudes of the (1, 0)-mode; the hollow symbols represent  $a_2$ , the amplitudes of the Faraday wave, the (0, 1)-mode.

almost symmetric about the minimum of the neutral stability curve. A  $180^\circ$  rotation of the cylinder did not affect either the orientation of the (1, 0)-mode or the regions in figure 3. We also note that the boundaries shown in figure 3 were reproducible, although the individual attractors in phase space for experiments within the boundaries were not always reproducible.

The region marked T (for threshold) in figure 3 contained wave fields that did not achieve an asymptotic behaviour. They typically grew for a few minutes and quickly died. Minutes later, they would recur, as though from a plane surface, and quickly die again. Hence, we could say nothing definitive about the long-term behaviour of waves in this region.

The waves in the region marked SS (for steady-state) had amplitudes that achieved steady values. Two experiments in this region had equilibrium amplitudes that suddenly jumped to new equilibrium amplitudes. Figure 5 shows the phase space, with modal amplitudes as the variables, for one such case. Here, the trajectory visited each fixed point for about three minutes. The modal amplitudes of the other experiments in this region are shown in figure 6 for different forcing amplitudes as a function of the corresponding Faraday-wave frequency. In general the wave amplitudes decreased as the frequencies increased and departed from the threshold

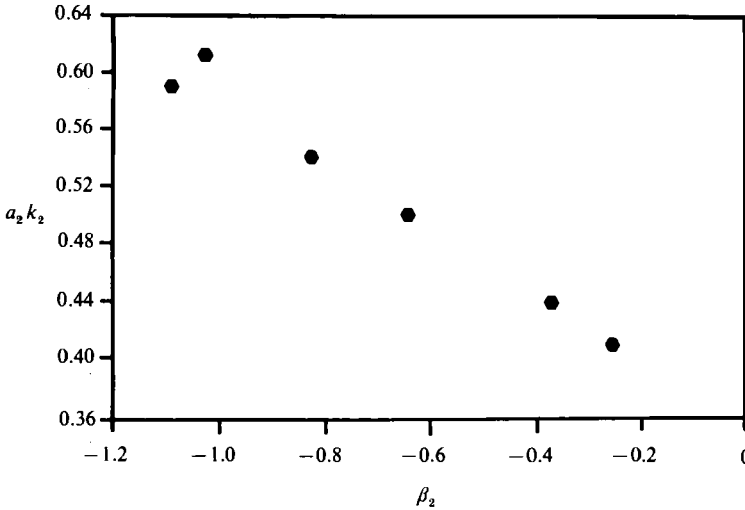


FIGURE 7. Measured wave slopes for the breaking waves corresponding to the hexagonal symbols in figure 3 as a function of the tuning parameter for the Faraday wave.

curve, toward the natural frequency. The Faraday wave usually had an amplitude less than that of its subharmonic; however, in some instances, such as in figures 6(c) and 6(d), these two roles were briefly reversed. Figures 6(c)–6(f) show that the amplitudes of the two modes seemed to converge as the frequencies approached  $f_2$ . For  $f < f_2$  the (1, 0)-mode reached a maximum amplitude of about 7 mm, which was close to the water depth of 7.6 mm. We remark that these wave fields were probably not in the putative range of validity of the weakly nonlinear theory. The predicted amplitudes for most of this parameter range are unstable to Hopf bifurcations and are smaller than those measured.

As indicated by the region marked B (for breaking) the steady waves ultimately reached a state for which the (0, 1)-mode wave started to break. We define breaking to mean that the (0, 1)-mode actually threw up drops of water. This definition is objective, since such behaviour is obvious to the eye and causes a high-frequency jitter to the otherwise steady time series; it does not include plunging or spilling waves. Figure 7 shows the slope of the (0, 1)-mode as a function of its frequency offset for the experiments located by the hexagonal symbols in figure 3. There appears to be a linear relationship between the slope and the frequency offset. For previous experiments on the (0, 1)-mode with no resonance present (Henderson & Miles 1990), the wave slopes were as large as 0.95 without breaking. The presence of an additional mode clearly affects the breaking criteria. We also note that the breaking waves are associated with steady-state motions, rather than chaotic motions.

Figure 8 shows some typical experimental results from the remaining four regions. (Note, these are representative experiments, not a sequence of experiments resulting from small increments in one of the parameters.) Here, column *e* shows the phase space with amplitudes as the coordinates; column *f* shows phase space with the (dimensional) amplitude of the cosine part of the time series; column *g* shows the power spectra of the attractor. (The spectra are computed from a time series of the total energy of the system equal to  $E_1(15a) + E_2(15b)$ ; the frequencies of the carrier waves are filtered out.) Columns *e* and *g* provide necessary information concerning the behaviour of the modal amplitudes. Column *f* does not provide obvious information

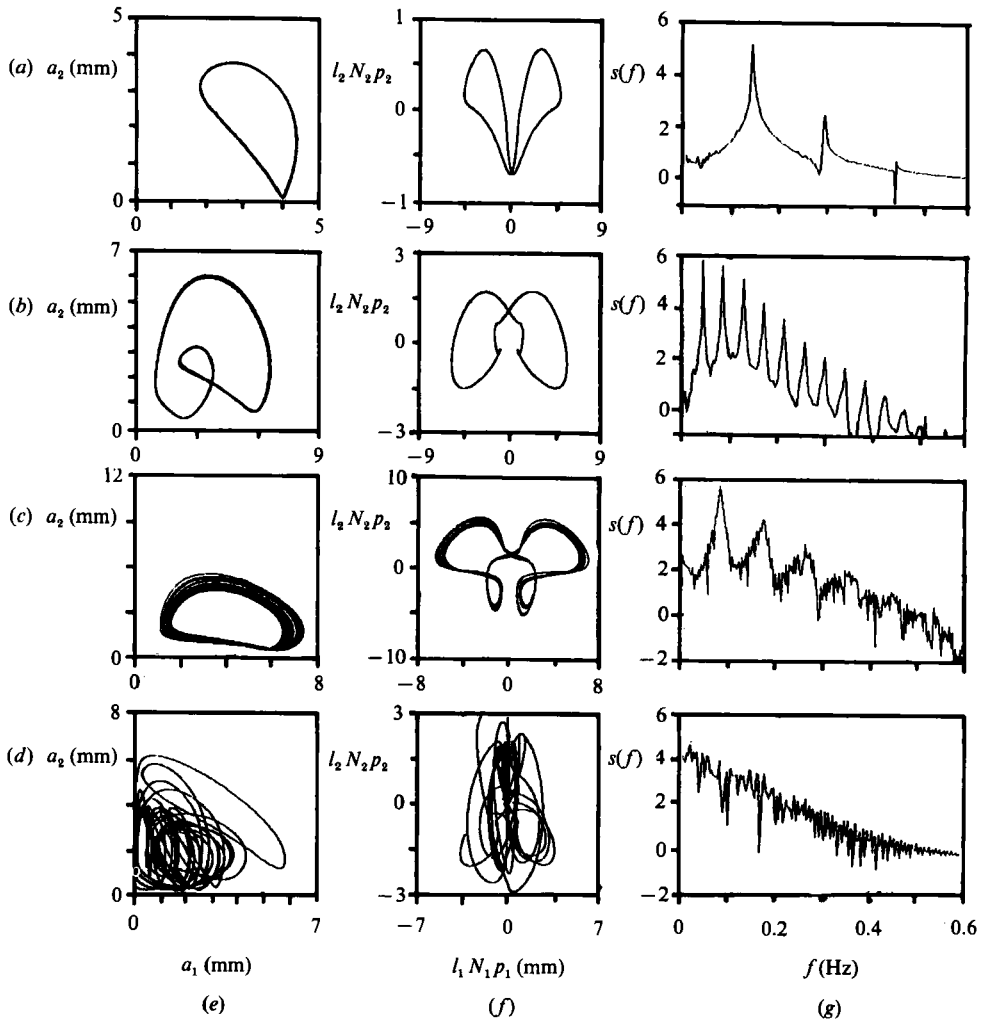


FIGURE 8. Representative measurements of phase-space trajectories and spectra for experiments in the SP region (row *a*:  $f_{0,1} = 4.182$  Hz,  $a_0 = 0.405$  mm), the DP region (row *b*:  $f_{0,1} = 4.164$  Hz,  $a_0 = 0.405$  mm), the Q region (row *c*:  $f_{0,1} = 4.164$  Hz,  $a_0 = 0.544$  mm) and the C region (row *d*:  $f_{0,1} = 4.255$  Hz,  $a_0 = 0.508$  mm) of figure 3. Column *e* contains the amplitude-phase space; column *f* contains the dimensional  $p$ -phase space; and column *g* contains the power spectra of the attractors.

on the behaviour of the modal amplitudes. Nevertheless, these attractors are of interest because they provide phase information that may be predicted, and because they are often symmetric about  $p_1 = 0$ .

Row *a* is a typical result from the region marked SP (for single period) of figure 3, where the modal amplitudes modulated with a single period. We note that the modulations of the fundamental followed those of the Faraday wave by about  $90^\circ$ . Ciliberto & Gollub (1984) also observed a  $90^\circ$  phase shift for 1:1 mode competition between the (7, 2)- and (4, 3)-modes in a circular cylinder. There is a limit cycle in amplitude-phase space, and the spectra is narrow-banded with one peak and its superharmonics. The attractor in  $p$ -phase space appeared for many of the wave fields, but a variety of other attractors also appeared. Figure 9 shows the measured frequencies of the limit cycles of all of the experiments in the SP region as a function

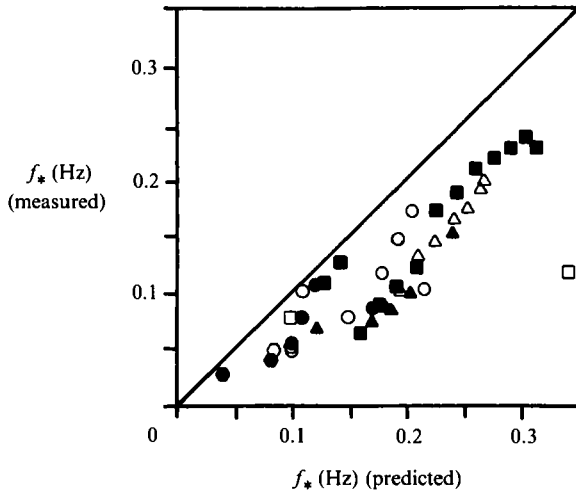


FIGURE 9. Measured and predicted frequencies of the limit cycles from the experiments in the SP region of figure 3. Each set of symbols represents experiments with given forcing amplitudes and different frequencies: ●,  $a_0 = 0.300$  mm; ○,  $a_0 = 0.334$  mm; ●,  $a_0 = 0.369$  mm; ○,  $a_0 = 0.405$  mm; △,  $a_0 = 0.442$  mm; ■,  $a_0 = 0.474$  mm; ▲,  $a_0 = 0.508$  mm; □,  $a_0 = 0.544$  mm.

of the limit-cycle frequency predicted by (16). The measured frequencies are spread consistently along the  $45^\circ$  line with a 0.5 Hz shift. In these calculations, we use the measured natural frequency of 4.135 Hz (the frequency corresponding to the minimum point in the measured neutral stability curve of figure 1). If we use the predicted value of 4.10 Hz, then predictions of limit-cycle frequencies are undefined for ten of the experiments. We remark that  $D$  (from 14c) is negative for these experiments, thus Hopf bifurcations and limit cycles are possible; however, numerical integrations of (7) using the experimental values for  $\alpha$  and  $\beta$  yield chaotic, rather than limit-cycle solutions.

Row  $b$  of figure 8 is a result from the region marked DP (for double period); in which the modal amplitudes exhibited period-doubling modulations. The result shown in row  $b$  is the best of the DP region in that the modulation amplitudes were constant during the measurement period, whereas the modulation amplitudes for other experiments in this region were not quite constant. (The diamonds outside the DP region represent additional experiments in which the (constant) modulation amplitudes had a double period.) Thus, many of the attractors in this region had finite widths not present for the one in row  $b$ . Nevertheless, all the waves in this region exhibited a double-looped limit cycle in amplitude-phase space, and the spectra showed that the frequencies of the attractors were in a 2:1 ratio. The attractor in  $p$ -phase space varied for each wave field.

Waves in the region marked Q (for quasi-periodic) exhibited three types of behaviour. Either they had single-period or double-period limit cycles with varying amplitudes (that still gave dominant peaks in the spectra), or (more rarely) they jumped from one attractor to some other attractor. Row  $c$  shows a case in which the wave-field amplitude modulated with a dominant periodicity that is evident in the spectrum. The modulation amplitude was not constant, thus the limit-cycle in amplitude-phase space has a finite width, as does the attractor in  $p$ -phase space. The final region of figure 3, marked C (for chaos), occurred along the boundary of the neutral stability curve for  $f > f_2$ . We note that much of this region is outside the

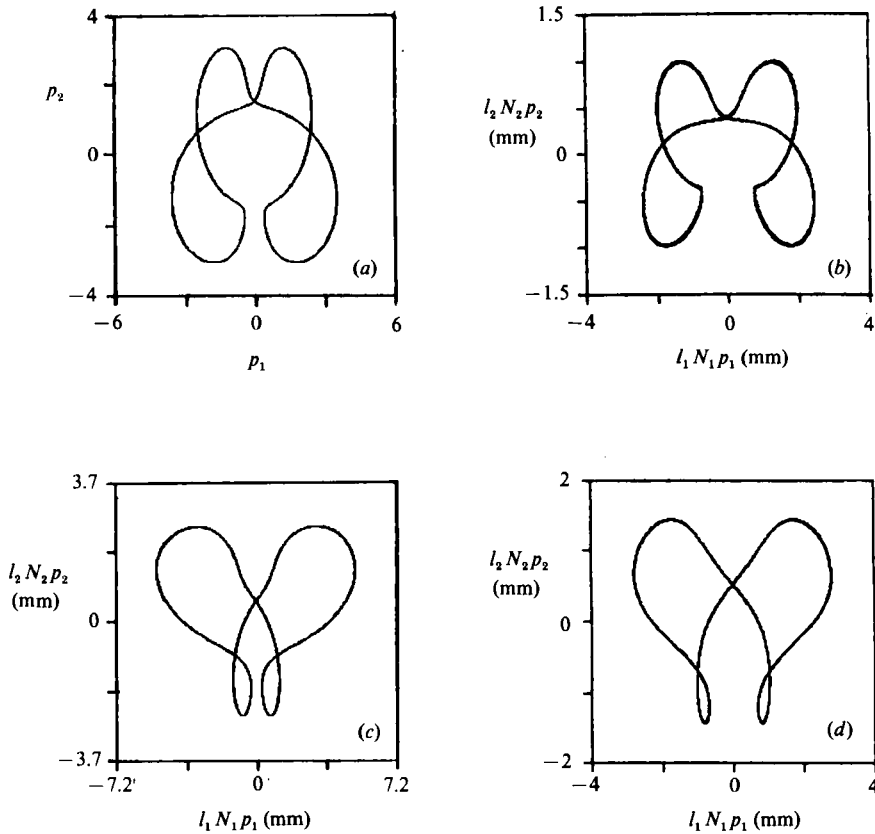


FIGURE 10.  $p$ -phase space from numerics and from experiments: (a) numerics:  $\alpha_1 = 1.444$ ,  $\alpha_2 = 0.962$ ,  $\beta_1 = -0.416$ ,  $\beta_2 = -1.177$ ; (b) experiments:  $\alpha_1 = 0.790$ ,  $\alpha_2 = 1.053$ ,  $\beta_1 = 0.685$ ,  $\beta_2 = 1.192$ ,  $a_0 = 0.508$  mm,  $f_{\text{forcing}} = 8.382$  Hz; (c) numerics:  $\alpha_1 = 0.991$ ,  $\alpha_2 = 1.321$ ,  $\beta_1 = 0.405$ ,  $\beta_2 = 0.582$ ; (d) experiments:  $\alpha_1 = 0.847$ ,  $\alpha_2 = 1.129$ ,  $\beta_1 = 0.670$ ,  $\beta_2 = 1.148$ ,  $a_0 = 0.474$  mm,  $f_{\text{forcing}} = 8.364$  Hz.

predicted neutral stability curve. A typical result from this region is shown in row  $d$  of figure 8. The trajectories in amplitude-phase space are beginning to fill up the phase space; the symmetry of the attractor in  $p$ -phase space is no longer apparent; and the spectrum is broadbanded without recognizable peaks. We calculated the largest Lyapunov exponent for data in the C region using the fixed-time evolution program of Wolfe *et al.* (1985). The exponents were positive, about 0.1 bit/s, but we were unable to establish any clear relationship with the frequency offset parameters.

The stability criteria of (14) predict that the fixed points of (12) and (13) should be stable near the threshold boundaries for  $f < f_2$  and  $f > f_2$ ; in between, Hopf bifurcations are possible. Although these predictions are not fully realized in the experiments, we can learn more from numerical integration of the evolution equations. Figures 10(a) and 10(c) show two examples of  $p$ -phase space trajectories from numerical integrations of (7), while figures 10(b) and 10(d) show similar trajectories from experiments. We note that the input parameters for the numerics and for the experiments are not the same; nevertheless, we show these results because of the similarities in the attractors. We did not calculate lengthscales for the numerical result of figure 10(a), since the damping parameters,  $\alpha_1$  and  $\alpha_2$ , could not correspond to experimental values. This attractor was first found by Becker & Miles (1986) for integrations of (7) with  $\alpha_1 = \alpha_2 = 1.0$  and  $\beta_1 = \frac{1}{2}\beta_2 = 0.48$ . The  $\alpha$  in figure

10(c) correspond to experiments with a forcing amplitude of  $a_0 = 0.405$  mm. We note that additional attractors found in the numerics were not observed in the experiments. Similarly, many attractors appeared in the experiments for which we found no theoretical counterparts.

## 5. Results of experiments on superharmonic resonance

We now describe the results of experiments on the resonance between a Faraday wave with frequency  $f$  and its superharmonic. We examined both low-mode and high-mode resonances. Table 2 lists the normal modes closest to resonance. Here the subscript 1 represents the normal mode of the Faraday wave, the subscript 2 represents the normal mode of its superharmonic, and the forcing frequency approximates  $f_2 = 2f_1$ .

### 5.1 *Low-mode superharmonic resonance*

To examine the possible resonance between a (0, 1)-mode and a (0, 3)-mode, we sequentially measured: (i) the neutral stability curve, (ii) time series for wave fields with a fixed forcing amplitude, but varying forcing frequency, and (iii) time series for wave fields with a fixed forcing frequency but varying forcing amplitudes. The measured neutral stability curve and the location of the additional experiments in stability space are presented in figure 11. We note that the theoretical curve slightly overpredicts the threshold amplitudes for all frequencies, but correctly predicts the natural frequency of the (0, 1)-mode.

Figure 12 shows time series of amplitudes of the Faraday wave and its superharmonic with a stretched interval (figure 12*b*) for the initial, transient region. This experiment corresponds to the first square symbol of figure 11. Resonance is observed here in the transient region of evolution as a phase shift between the two modes. As in the experiments of §4.2 and those of Ciliberto & Gollub (1984), the phase shift is about  $90^\circ$ . (In non-resonant experiments, the superharmonic always had the same phase as the fundamental.) The waves quickly stopped the low-frequency modulations and developed a high-frequency modulation that was due to a precession instability of the (0, 1)-mode. Figure 13 shows a sample of the precession instability for the experiment corresponding to the second triangle in figure 11. This higher-frequency modulation retained the phase shift observed in the transient region, as well as its lower-frequency modulation.

As frequency was increased along the square symbols in figure 11, the initial modulations of the modal amplitudes became more in phase; at  $f = 4.639$  Hz the modulations were in phase. This wave field was the one that most closely corresponded to the theoretical 2:1 resonance. The amplitudes and durations of the initial modulations began to lessen as the frequency further increased along the square symbols, until at the last symbol, at threshold, no initial modulations were present. In addition, as frequency was increased along the square symbols, the magnitude of the precession instability decreased and disappeared at  $f = 4.596$  Hz. When the frequency was fixed and the forcing amplitude was increased, the precession instability either occurred or became stronger, and the duration of the initial modulations increased.

We believe that the observed phase shift between the modulations of the two modes is evidence of the 2:1 resonance. However, we note that the modulations last only tens of seconds and that the amplitude of the superharmonic never becomes comparable with that of the fundamental.

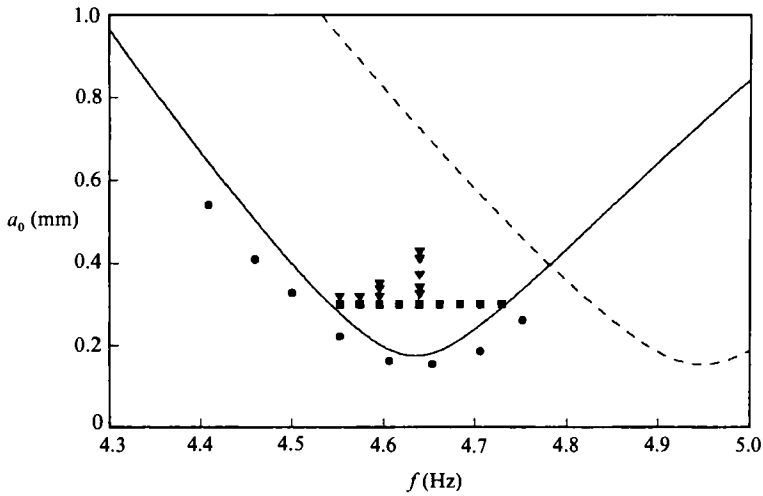


FIGURE 11. Stability space of forcing amplitude as a function of the (0, 1)-mode Faraday-wave's frequency for experiments on low-mode superharmonic resonance with  $h = 1.15$  cm; —, predicted and ●, measured neutral stability curve of the (0, 1)-mode; ---, predicted neutral stability curve of the (3, 0)-mode; ■, location of experiments with  $a_0 = 0.300$  mm; ▼, location of additional experiments.

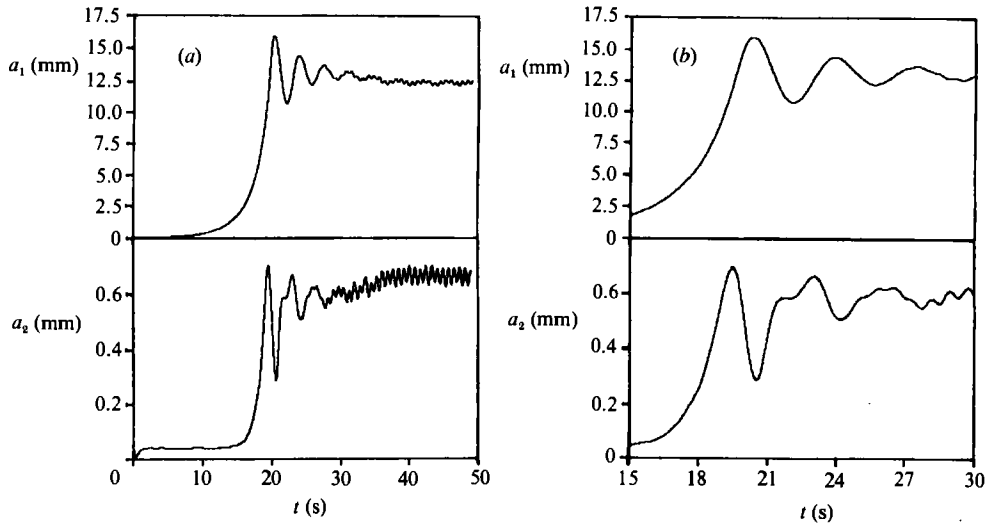


FIGURE 12. Time series of the amplitudes of the Faraday wave and its superharmonic (a), with a close-up of the transient region (b):  $f_{0,1} = 4.553$  Hz,  $a_0 = 0.300$  mm.

$h$ (cm)	$k_1$ /(mode) (rad/cm)	$f_1$ (Hz)	$\delta_1$	$k_2$ /(mode) (rad/cm)	$f_2$ (Hz)	$\delta_2$	$\nu_{\text{effective}}$ (cm <sup>2</sup> /s)
1.15	1.03 (0, 1)	4.64	0.015	2.74 (0, 3)	9.28	0.018	0.016
2.04	3.47 (7, 1)	11.12	0.029	6.95 (0, 8)	22.24	0.037	0.030

TABLE 2. Parameters and normal modes for the experiments on superharmonic resonance. The subscript 1 indicates the parameter appropriate for the normal mode of the Faraday wave. The subscript 2 indicates the parameter appropriate for the normal mode of its superharmonic.

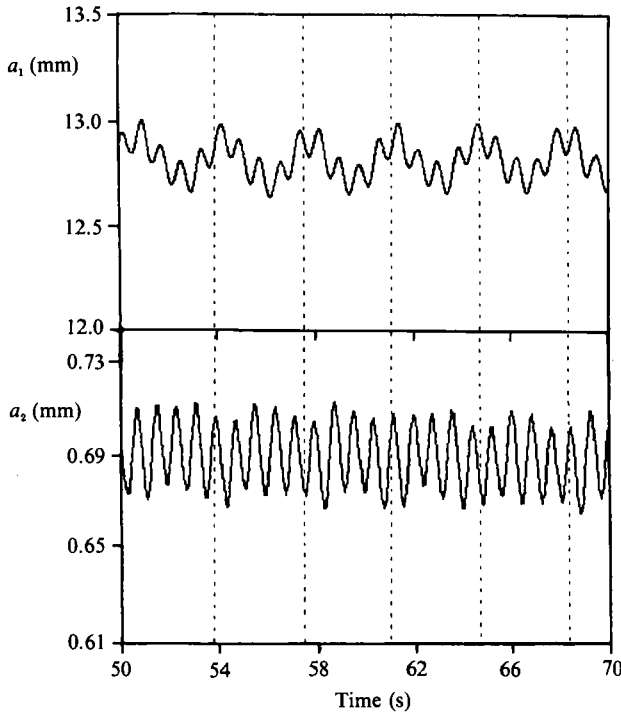


FIGURE 13. Time series of the amplitudes of the Faraday wave and its superharmonic during a precession instability:  $f_{0,1} = 4.574$  Hz,  $a_0 = 0.320$  mm.

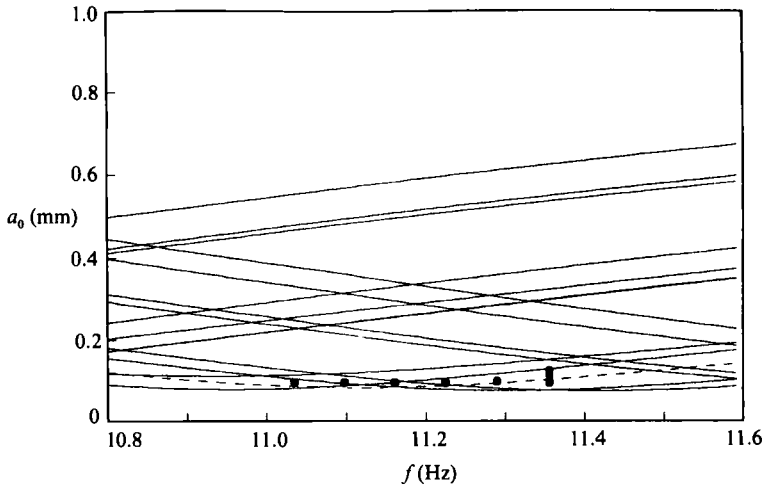


FIGURE 14. Stability space of forcing amplitude as a function of the Faraday wave frequency for experiments on high-mode superharmonic resonance with  $h = 2.040$  cm; —, predicted neutral stability curves of the normal modes near the resonant one; ---, neutral stability curve for the normal mode most closely approximating 2:1 resonance; ●, location of experiments.

*5.2. High-mode superharmonic resonance*

The experiments discussed in this section are a standing-wave analog of Wilton's ripple (Wilton 1915), for which a progressive wave in deep water has a superharmonic whose frequency and wavenumber satisfy the linear dispersion relation (1), are in a

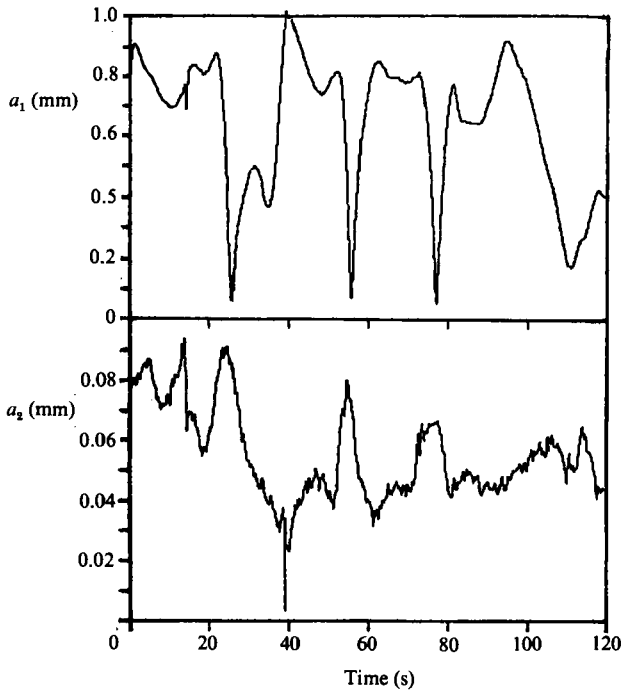


FIGURE 15. Time series of the amplitudes of the Faraday wave and its superharmonic with  $h = 2.040$  cm;  $f_{7,1} = 11.355$  Hz and  $a_0 = 0.098$  mm.

2:1 ratio with the fundamental, and are thus able to resonate. Previous experiments on progressive Wilton's ripples (e.g. McGoldrick 1970) were hampered by viscous effects. Hence, our objective was to examine Wilton's ripple in a standing-wave system, in which viscosity would enter the calculation for the normal modes and evolution equations, but would not detune the normal modes during evolution. The experimental parameters and normal modes for the present experiments that most closely approximate Wilton's ripple are listed in table 2.

Figure 14 shows the location in stability space of the high-mode experiments. The density of curves shows that many spatial modes exist that have frequencies close to that of the calculated frequency for resonance. When the wave fields were steady, the amplitude of the superharmonic was an order of magnitude smaller than that of the fundamental (as also was true for non-resonant cases). When the wave fields were unsteady, the modulations of the superharmonic were often out of phase from those of the fundamental. This phase shift, which is not present for non-resonant waves, indicates an energy exchange between the two modes; as the subharmonic mode loses amplitude, its superharmonic gains amplitude and vice versa. Figure 15 shows the best measurement of the energy exchange. Note that the phase shift is  $180^\circ$ , unlike the experiments from §4.2 and §5.1, where the phase shift was  $90^\circ$ . The  $180^\circ$  shift is predicted by resonant interaction theory (e.g. Simmons 1969) for the energy exchange between Wilton's ripple and its superharmonic. We emphasize that this energy exchange was transient and not reproducible for particular forcing parameters. As the forcing amplitude was increased and many Faraday-wave modes were present, the modal amplitudes of the two waves modulated randomly, sometimes in phase, sometimes not. As with the steady waves, the amplitude of the superharmonic never became comparable with that of the fundamental.

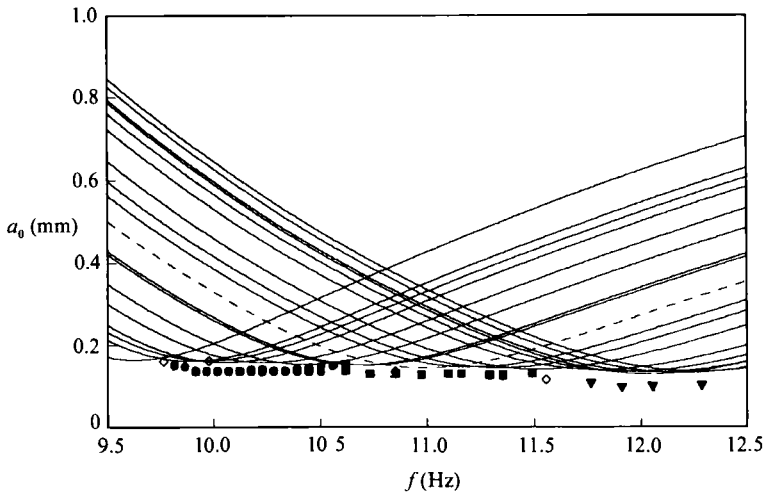


FIGURE 16. Stability space of forcing amplitude as a function of the Faraday wave frequency for experiments on high-mode superharmonic resonance in the rectangular container with  $h = 0.750$  cm; —, predicted neutral stability curves of the normal modes near the resonant one; ---, neutral stability curve for the normal mode most closely approximating 2:1 resonance; location of experiments for ●, the (9, 0)-mode ■, the (10, 0)-mode ▼, the (11, 0)-mode and ◇, multiple modes.

$h$ (cm)	$k_1$ /(mode) (rad/cm)	$f_1$ (Hz)	$\delta_1$	$k_2$ /(mode) (rad/cm)	$f_2$ (Hz)	$\delta_2$	$\nu^{\text{effective}}$ (cm <sup>2</sup> /s)
0.75	3.54 (10, 0)	10.99	0.051	7.08 (20, 0)	22.01	0.067	0.10

TABLE 3. Parameters and normal modes for the experiments on superharmonic resonance in the rectangular cylinder. The subscript 1 indicates the parameter appropriate for the normal mode of the Faraday wave. The subscript 2 indicates the parameter appropriate for the normal mode of its superharmonic.

### Appendix. Experiments on superharmonic resonance in the rectangular cylinder

For a rectangular cylinder with cross-sectional area  $ab$ , the wavenumber of the  $(l, m)$ -mode,  $k_{lm} \equiv [(l\pi/a)^2 + (m\pi/b)^2]^{1/2}$ , is related to the frequency by (1). For superharmonic resonance  $f_2 = 2f_1$ , and  $k_2 = k_{2l2m}$  must equal  $2k_1 = 2k_{lm}$ ; hence, superharmonic resonance in a rectangular cylinder is always analogous to Wilton's ripple. For surface waves, this situation is possible only if surface tension is a restoring force; hence, superharmonic resonance is not possible for gravity waves in a rectangular cylinder. For the rectangular cylinder used here with cross-sectional dimensions of 8.870 cm  $\times$  3.205 cm, superharmonic resonance was only possible for high modes. The experimental parameters and normal modes most closely approximating resonance are given in table 3.

Figure 16 shows the location in stability space of the experiments. A broad band of frequencies was investigated for wave fields in the rectangular geometry because the determination of the damping rate for this geometry (and thus for the resonant normal modes) was more uncertain than it was for waves in the circular cylinder (see Henderson & Miles 1990). We note that in these experiments the wave field was

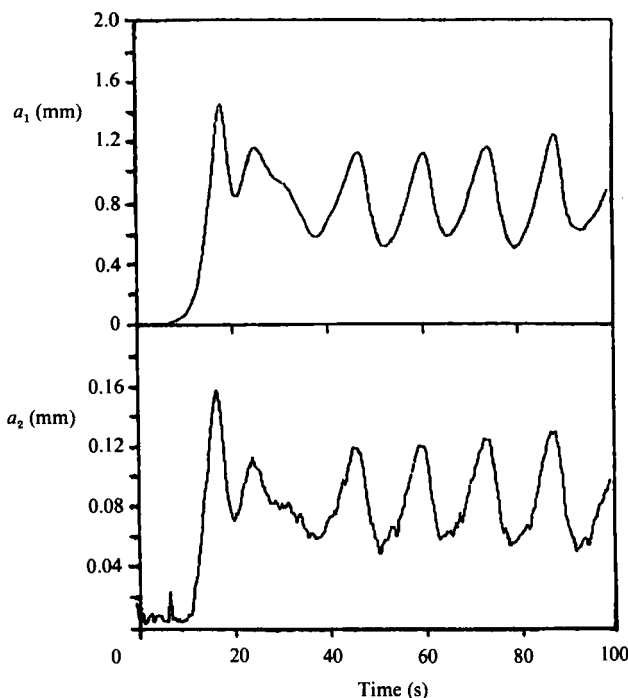


FIGURE 17. Time series of the amplitudes of the Faraday wave and its superharmonic in the rectangular cylinder with  $h = 0.750$  cm;  $f_{10,0} = 10.731$  Hz,  $a_0 = 0.131$  mm.

usually a one-dimensional mode, although many two-dimensional modes were available for excitation. The single-mode, (9, 0)- and (11, 0)-mode, wave fields were usually steady, with the amplitude of the superharmonic an order of magnitude less than that of the fundamental. Multi-mode wave fields were often modulated; the wave field periodically alternated between two (Faraday) modes, and the location of the wave gauge alternated between anti-node and node. (See Cililberto & Gollub (1985) for experiments on 1:1 mode competition of waves in a circular cylinder.) Many of the (10, 0)-mode wave fields also exhibited modulations. In these experiments the (10, 0)-mode seemed to decay and grow periodically. Figure 17 shows an example of these modulations. Note that the superharmonic is in phase with the fundamental; hence, we do not believe these modulations are the result of superharmonic resonance. The most likely explanation appears to be 1:1 mode competition, although no other mode was visible during the decay part of the cycle. Two gauges would be needed to verify this conjecture. In brief, we did not observe the phase shift expected from a resonant interaction in any of the experiments conducted in the rectangular cylinder.

This work was supported in part by the Physical Oceanography, Applied Mathematics and Fluid Dynamics/Hydraulics programs of the National Science Foundation, NSF Grant OCE-85-18763, by the Office of Naval Research, Contract N00014-84-K-0137, 4322318 (43), by the DARPA Univ. Res. Init. under Appl. and Comp. Math Program Contract N00014-K-0758 administered by the Office of Naval Research.

## REFERENCES

- BECKER, J. & MILES, J. 1986 Parametric excitation of an internally resonant double pendulum, II. *Z. angew. Math. Phys.* **37**, 641–650.
- BECKER, J. & MILES, J. 1991 Standing radial cross-waves. *J. Fluid Mech.* **222**, 471–499.
- BLOOMFIELD, P. 1976 *Fourier Analysis of Time Series: An Introduction*. Wiley.
- CILIBERTO, S. & GOLLUB, J. P. 1984 Pattern competition leads to chaos. *Phys. Rev. Lett.* **52**, 922–925.
- CILIBERTO, S. & GOLLUB, J. P. 1985 Chaotic mode competition in parametrically forced surface waves. *J. Fluid Mech.* **158**, 381–398.
- CONCUS, P. 1962 Standing capillary-gravity waves of finite amplitude. *J. Fluid Mech.* **14**, 568–576.
- GOLLUB, J. P. & MEYER, C. W. 1983 Symmetry-breaking instabilities on a fluid surface. *Physica* **6(D)**, 337–346.
- GU, X. M. & SETHNA, P. R. 1987 Resonant surface waves and chaotic phenomena. *J. Fluid Mech.* **183**, 543–565.
- HENDERSON, D. M. & MILES, J. W. 1990 Single-mode Faraday waves in small cylinders. *J. Fluid Mech.* **213**, 95–109.
- MCGOLDRICK, L. F. 1970 On Wilton's ripples: a special case of resonant interactions. *J. Fluid Mech.* **42**, 193–200.
- MILES, J. W. 1967 Surface-wave damping in closed basins. *Proc. R. Soc. Lond. A* **297**, 459–475.
- MILES, J. W. 1984 Nonlinear Faraday resonance. *J. Fluid Mech.* **146**, 285–302.
- MILES, J. & HENDERSON, D. 1990 Parametrically forced surface waves. *Ann. Rev. Fluid Mech.* **22**, 143–165.
- PHILLIPS, O. M. 1977 *The Dynamics of the Upper Ocean*, 2nd edn. Cambridge University Press.
- SIMMONS, W. F. 1969 A variational method for weak resonant wave interactions. *Proc. R. Soc. Lond. A* **309**, 551–579.
- SIMONELLI, F. & GOLLUB, J. P. 1989 Surface wave mode interactions: Effects of symmetry and degeneracy. *J. Fluid Mech.* **199**, 471–494.
- TADJBAKHSH, I. & KELLER, J. B. 1960 Standing surface waves of finite amplitude. *J. Fluid Mech.* **8**, 442–451.
- WILTON, J. R. 1915 On ripples. *Phil. Mag.* **29** (6), 688–700.
- WOLFE, A., SWIFT, J. B., SWINNEY, H. L. & VASTANO, J. A. 1985 Determining Lyapunov exponents from a time series. *Physica* **16(D)**, 285–317.